START-TO-END BEAM DYNAMIC SIMULATIONS FOR FEMTO-SCIENCE-FACTORY FEASIBILITY STUDY*

T. Atkinson†, A. Bondarenko, A. Matveenko, Y. Petenev,
Helmholtz-Zentrum Berlin für Materialien und Energie GmbH (HZB), Germany.

Abstract

Design studies for a future multi-turn ERL based light source at HZB are being investigated. The Femto-Science-Factory will provide its users with ultra-bright photons of angstrom wavelength at 6 GeV. The FSF is intended to be a multi-user facility and offer a wide variety of operation modes. A low emittance $\sim 0.1\,\mu$m rad mode will operate in conjunction with a short-pulse $\sim$10 fs mode. This paper reports on the first results of the start-to-end beam dynamic simulations for both modes. Higher order geometric and chromatic aberration terms have been suppressed using both multipole magnets and biased off-crest acceleration. The influence of the collective effects (coherent synchrotron radiation) on the transversal emittance is minimised by adjusting the horizontal phase advance.

INTRODUCTION

This paper continues on from a recent Analysis of Injection and Recovery study[1] for Multi-turn ERL based light sources and highlights the physical limitations when trying to offer interchangeable modes and preserve beam quality.
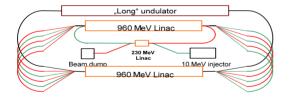

Figure 1: Schematic of the FSF Multi-Turn ERL.

The main design parameters of the FSF are listed in Table 1 and Fig. 1 shows the layout of the light source. In this scheme the acceleration of the whole FSF is constrained to be scalable. This modification relaxes the design of the vertical spreaders, so that if the energy is changed, due to possible upgrades or unforeseen circumstances one would simply adjust the field gradient in the cavity rather than redesign the spreader. Using the scaling formula $E_f = (1+2kN)(E_i+E_{pre})$, an SRF injector based on the design parameters of BERLinPro[2], injects the $E_i = 10\,MeV$

Table 1: Main design parameters of FSF

Parameter	Low Emittance Mode	Short Pulse Mode
Preinjector (MeV)	230	
Main Linacs (MeV)	960	
Final Energy (GeV)	6	
Charge (pC)	15	4
Emittance (mm mrad)	0.1	0.4
Bunch Length (fs)	2000	10

electron beam into a $E_{pre} = 230\,MeV$ preinjector accelerator. From here onwards two equally long linacs are continually traversed each with $N = 3$ passes until the $E_f = 6\,GeV$ final beam energy is reached. Choosing a suitable value $k = 4$ sets the main linacs to both $960\,MeV$.

Each Arc contains straight sections for undulators and in the final energy Arc 3000 period long of 40 mm period length undulators are foreseen.

The higher energy injection into the independent orbit ERL recirculator has naturally modified the beam dynamics from previous studies[3]. The new optic in the linacs has been optimised for the highest Beam Break Up threshold[1]. In this paper the remaining optic with regards to transversal and longitudinal emittance growth are discussed.

TRANSVERSAL EMITTANCE PRESERVATION

The difference in the two modes with regards to the lattice design occurs in the low energy section of the machine. For the Low Emittance Mode (LEM) a beam of higher charge is accelerated on crest in all of the linacs and circulates round isochronous Arcs. The Short Pulse Mode (SPM) however relies on achromatic arcs for the telescopic compression technique[3] removing the correlated energy spread due to the off-crest acceleration. The modes share common high energy arcs where radiation effects play an important role in emittance growth and will be firstly addressed.

High Energy Arcs

Consider the geometrical parameters of Coherent Synchrotron Radiation (CSR) as described in [4]. Taking the

FSF beam properties, the characteristic radiation length a, is smaller than the deviation of the tangent from the circulating beam at the overtaking distance L_t, and with it the vacuum chamber diameter D, $a < L_t < D$, hence a 1D model without shielding will suffice [5]. The transversal CSR shift $(\delta x, \delta x')$ depends only on the longitudinal bunch profile and the slice coordinate.

For two consecutive identical isochronous bends, the longitudinal bunch shape does not change and the bunch dynamics are identical if the additional relative energy spread δ_{CSR} due to CSR produced in the first bend is small enough in the chosen dispersive section, hence $\delta_{CSR} R_{56} << \sigma_z$. Let the bends have a horizontal transformation matrix M_x. In the first bend, particles experience shifts δx and $\delta x'$ due to CSR. In the second bend these deviations undergo betatron oscillations and exactly the same shifts δx and $\delta x'$ are simply added Eq. 1 to them once more.

$$\begin{pmatrix} \delta x \\ \delta x' \end{pmatrix}_2 = \begin{pmatrix} \delta x \\ \delta x' \end{pmatrix}_0 + M_x \begin{pmatrix} \delta x \\ \delta x' \end{pmatrix}_0 \qquad (1)$$

$$= \left(I(1 + cos\mu_x) + J sin\mu_x) \right) \begin{pmatrix} \delta x \\ \delta x' \end{pmatrix}_0$$

If the betatron phase $\mu_x = \pi$ the impact of CSR on the transversal emittance is null[6]. The same effect can be achieved for a system of N identical isochronous bends. The CSR shift is then given by Eq. 2.

$$\begin{pmatrix} \delta x \\ \delta x' \end{pmatrix}_N = \sum_{n=0}^{N} M_x^n \begin{pmatrix} \delta x \\ \delta x' \end{pmatrix}_0 \qquad (2)$$

$$= \left(I \sum_{n=0}^{N} cos(n\mu_x) + J \sum_{n=0}^{N} sin(n\mu_x) \right) \begin{pmatrix} \delta x \\ \delta x' \end{pmatrix}_0$$

Now if $\mu_x = 2\pi \cdot k/N$ where k is an integer, the impact of CSR on the transversal emittance is again nullified.
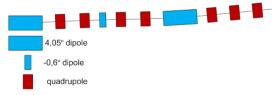

4,05° dipole

-0,6° dipole

quadrupole

Figure 2: Schematic of a cell with anti-magnet.

Consider a $7.05°$ cell of a $30°$ bend as shown in Fig. 2. Here long dipoles (blue) of bending angle $4.05°$ are separated by quadrupoles (red) and a short $-0.6°$ bend anti-magnet dipole (also blue) that keeps the quadrupole strength low (no need to actively change the sign of the dispersion to ensure $R_{56} = 0$). Fig. 3 shows the beta-functions for a $30°$ bend of horizontal phase advance $\mu_x = 2\pi \cdot 3/4$. There are four quadrupoles at each end to match the twiss parameters to those needed for the undulator sections between the Arcs.

When simulating a $15\,\text{pC}$, $10\,\text{fs}$ input bunch using CSRtrack[7] the relative energy spread δ_{CSR} produced in
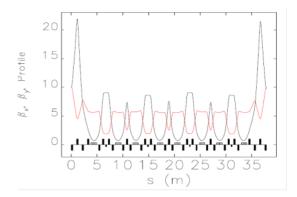

Figure 3: Beta functions in the $30°$ bend.

one cell can be estimated[8] as $\delta_{CSR} \sim q/\sigma_z^{4/3} \sim 10^{-4}$ and is depicted in Fig. 4. The emittance growth from each $7.5°$ bending cell is almost fully compensated Fig. 5 for a $30°$ Arc.
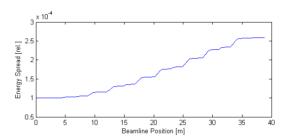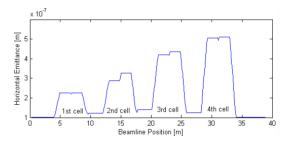

Figure 4: Relative energy spread along the $30°$ bend.

Figure 5: Normalised transversal emittance along the $30°$ bend.

The bends described have been implemented into the FSF optic of the $180°$ High Energy Arcs. It has been found however that especially for the short pulse mode, the second order aberrations also play a significant role in the causes of emittance growth, the next section describes the suppression techniques currently being investigated.

2nd Order Aberrations

Rather than using multipoles to manipulate "all" the higher matrix terms in order to optimise the chromatic dependence of the phase advance; $\xi = \Delta\xi/(\Delta p/p)$ the transfer line chromaticity, a simpler approach has been undertaken to find the key 2nd order terms which stimulate

traversal emittance growth. Consider the chromatic aberrations in the horizontal plane given by Eq. 3.

$$x_1 = T_{161}\delta_0 x_0 + T_{162}\delta_0 x_0' + ... \qquad (3)$$
$$x_1' = T_{261}\delta_0 x_0 + T_{262}\delta_0 x_0' + ...$$

Using these linear terms of the chromatic aberration, one can approximate the emittance change as Eq. 4.

$$\varepsilon_x^2 = <x_1^2><x_1'^2> - <x_1 x_1'>^2 \qquad (4)$$
$$= <(T_{161}\delta x + T_{162}\delta x')^2><(T_{261}\delta x + T_{262}\delta x')^2>$$
$$- <(T_{161}\delta x + T_{162}\delta x')(T_{261}\delta x + T_{262}\delta x')>^2$$

many like terms simply cancel out

$$\varepsilon_x^2 = \Big\{ (T_{161}^2 T_{261}^2 + T_{162}^2 T_{261}^2) <\delta^2 x^2><\delta^2 x'^2>$$
$$+ 4T_{161}T_{162}T_{261}T_{262} <\delta^2 xx'>^2$$
$$-$$
$$+ 2T_{161}T_{162}T_{261}T_{262} <\delta^2 x^2><\delta^2 x'^2>$$
$$+ (T_{161}T_{262} + T_{162}T_{261})^2 <\delta^2 xx'>^2 \Big\}$$

$$\varepsilon_x^2 = (T_{161}T_{262} - T_{162}T_{261})^2 *$$
$$\big\{ <\delta_0^2 x_0^2><\delta_0^2 x_0'^2> - <\delta_0^2 x_0 x_0'>^2 \big\} \qquad (5)$$

One can interpret Eq. 5 as a useful tool to suppress the transverse emittance growth. By implementing two families of sextupoles so that for the horizontal plane $T_{161}T_{262} = T_{162}T_{261}$ and likewise for the vertical plane $T_{363}T_{464} = T_{364}T_{463}$ the magnitude of the chromatic emittance growth is dramatically reduced.
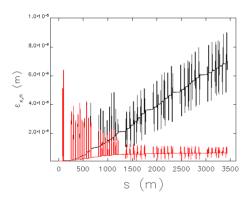

Figure 6: Correction of the 2nd order aberrations.

Fig. 6 demonstrates this concept over the complete 3.5 km long acceleration stage of the FSF to the long undulator section, with a chromatic perturbation in the preinjector Arc. The curves shown are both for the horizontal plane, the wavering effect due to the dispersion show the six Arcs and between them the linac sections. The Arcs

containing sextupoles (red) using Eq. 5 reduce the emittance growth due to 2nd order aberrations in this example for the short pulse mode by almost a magnitude.

This new approach gives comparable results to standard chromaticity optimisation techniques but more importantly relaxes the restrictions on other essential 2nd order terms such as T_{566} which are additionally optimised to aid the longitudinal dynamics during bunch compression.

LONGITUDINAL EMITTANCE PRESERVATION

The longitudinal emittance compensation scheme first described in [3] uses the higher order magnetic terms created in the Arc and the off-crest acceleration Eq. 8 to recover the longitudinal emittance of the injector. Using the linacs relative energy Eq. 6 and the Arcs bunch length Eq. 7 variations respectively one can calculate the emittance variation across the two stages as follows.

$$LINAC$$
$$\delta_1 = \delta_0 + R_{65}c\Delta t_0 + T_{655}(c\Delta t_0)^2 \qquad (6)$$
$$c\Delta t_1 = c\Delta t_0$$

$$+ARC$$
$$\delta_2 = \delta_1$$
$$c\Delta t_2 = c\Delta t_1 + R_{56}\delta_1 + T_{566}\delta_1^2 \qquad (7)$$

Keeping only second order terms, assuming $\delta_0 = 0$ and substituting Eq. 6 and Eq. 7 the emittance can be approximated as Eq. 8

$$\epsilon_z^2 = <(c\Delta t_2)^2><\delta_2^2> - <(c\Delta t_2\delta_2)>^2 \qquad (8)$$
$$\epsilon_z^2 = \big(T_{566}R_{65}^3 - T_{655}\big)^2 <(c\Delta t_0)^4><(c\Delta t_0)^2>$$

The accelerating phase ϕ determines both the R_{65} and T_{655} terms and sextupoles in the Arc can adjust T_{566} to compensate longitudinal emittance growth. Fig. 7 shows the recovery of normalised longitudinal emittance (black) using sextupoles in the first two Arcs with the optimum T_{566} for the given linac phase.

The emittance then slowly starts to increase (between s=1→6 km) due to radiation effects producing the unwanted energy spread. Shown also is the bunch length (red) along the whole machine. The logarithmic plot (where 15→1 fs), shows an optic producing a bunch length of less then 10 fs at the long undulator section at the half way point along the machine.

The optimum T_{566} setting is extremely sensitive to the linac phase setting Eq. 9 and only technical feasible values for T_{566} are produced for off crest acceleration, hence the main linacs in the SPM are +10° and -20° respectively.

$$T_{566} = \frac{T_{655}}{R_{65}^3} \sim \frac{c}{2\omega}\left(\frac{E}{\Delta E}\right)^2 \frac{1}{\phi^3} \qquad (9)$$
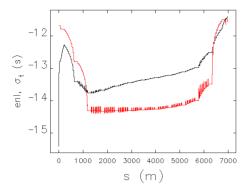
Figure 7: Log plot of the longitudinal bunch properties.

Each off-crest acceleration is followed by achromatic Arcs of positive R_{56} values constitute the telescopic compression scheme in the lower energy acceleration sections.
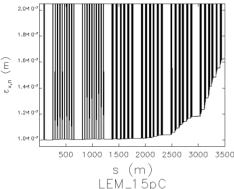
AT THE LONG UNDULATOR

Figure 8: Normalised horizontal emittance during the acceleration stage for the LEM.

Table 2: Simulation results at long undulator entrance

Type	ε_{nx} (mm mrad)	ε_{ny} (mm mrad)	St (fs)	$\Delta E/E$ (10^{-4})	Charge (pC)
Input	0.10	0.10	2000	0.10	Gaussian
SPM	0.22	0.11	6	10.2	1
SPM	0.21	0.10	20	7.01	5
LEM	0.16	0.10	2000	1.96	15

The machine optic was optimised independent of input bunch parameters. The first results from tracking a low emittance Gaussian input bunch to the long undulator are given in Table 2 and compare well with the expectations Table 1 of a high brilliance light source.

For the low emittance mode Fig. 8, with all the suppression techniques previously described in place, the transversal emittance mainly grows due to classical radiation effects and can be analytically estimated using the integral Eq. 10 of the 6 GeV Arc. One can then cross reference the emittance growth by simply using Eq. 11.

$$I_5 = \int \frac{H}{|\rho|^3} ds \sim 2 \cdot 10^{-5} \tag{10}$$

$$\Delta(\gamma\varepsilon) \simeq 4 \cdot 10^{-8} E^6 I_5 = 0.04 \, \text{mm mrad} \tag{11}$$

START-TO-END

Injection

Producing a 6D ultra low emittance bunch to match the FSF parameter expectations remains an essential part of this and many other future projects. ASTRA[9] simulations from the photo-injector, through the Booster and Merger to the preinjector linac remain ongoing.

Table 3: Injector ASTRA simulations

Pos.	ε_{nx} (mm mrad)	ε_{ny} (mm mrad)	ε_z (keV mm)	Ss (mm)	$\Delta E/E$ (10^{-4})	Energy (MeV)
Gun	0.15	0.15	0.40	0.65	2.10	2.80
Booster	0.16	0.16	1.20	0.67	3.10	10.0
Merger	0.28	0.18	1.17	0.70	3.79	10.0

Table 3 shows a subtle beam transformation through the space charge dominated injection process to produce a low emittance beam in all dimensions.
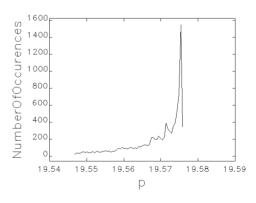

Figure 9: Energy distribution of input beam at 10 MeV.

Fig. 9 reiterates the very low rms energy spread for this input file. These beam distributions are then converted, matched and tracked onwards using Elegant[10].

A possible scenario to make good use of each 50 m long transfer line between the 230 MeV preinjector and Arcs is

to envisage optic that may be used at a future date to aid the non-linear beam dynamics. For instance on the acceleration side, green in Fig. 1, a series of Laser Heater undulators could be implemented and used to suppress the micro-bunching instability at the expense of the longitudinal emittance. Such a scheme could based on [11] where a TiSa laser is used to overlap and interact with the electron beam.

$$\lambda = \frac{d}{2\gamma^2}(1 + \frac{K^2}{2}) \qquad (12)$$

Considering Eq. 12, a laser wavelength of $\lambda = 800\,nm$ and common undulator parameters are suitable for interaction at this relatively low energy stage ($\gamma = 480$).

On the deceleration side, an optic based on a pseudo-reflector[12] (rotator) could be included to interchange the x-y motion. Such a rotation in bunch coordinates has been theoretically shown to suppress beam breakup and increase the threshold current in the preinjector linac.

Energy Loss Considerations

It is envisaged that the total energy loss due to radiation in the Arcs alone will exceed the 10 MeV injection energy of the FSF. Considering the contribution from ISR using Eq. 13 in each Arc of bending radius R.

$$U\,[MeV] = 0.088E^4\,[GeV]/R\,[m] \qquad (13)$$

The total energy loss due to ISR alone is 15 MeV. In a similar manner, the total energy loss due to ISR in the abundance of undulators can be calculated using Eq. 14.

$$U\,[keV] = 0.633E^2\,[GeV]B^2[T]L[m] \qquad (14)$$

Given the present undulator parameters, this amounts to an energy loss of 6.4 MeV during acceleration. These values coupled with the addition of energy loss due to CSR ΔE_{CSR} far exceeds an injection energy of 10 MeV. Using the rectangular bunch[13] model the ΔE_{CSR} per turn can be approximated as Eq. 15.

$$\Delta E_{CSR} \simeq -\Big(\frac{3^{\frac{2}{3}}e^2N^2}{l_b^{\frac{4}{3}}R^{\frac{2}{3}}}\Big)(R\phi_m)*$$

$$\Big(1 + \frac{3^{\frac{1}{3}}4}{9}\frac{l_b^{\frac{1}{3}}}{R^{\frac{1}{3}}\phi_m}\Big[\ln\Big(\frac{l_b\gamma^3}{R}\Big) - 4\Big]\Big) \qquad (15)$$

The contribution in the LEM is negligible compared to that of the SPM which is given in Table 4 for different bunch charge.

Table 4: Energy loss due to radiation, acceleration stage

SPM	ISR		CSR	
	Arc	Und.	1 pC	5 pC
Energy loss (MeV)	15.5	6.4	3.3	16.4

Booster modules were implemented in the simulations to compensate for this energy loss due to radiation. These modules operate without energy recovery and require approximately 300 kW and 200 kW of power for the LEM and SPM respectively.

Low Emittance Mode

The transverse emittance growth is kept to a minimum throughout the whole 7 km machine, Fig. 10 to utilize the undulator radiation in all acceleration and deceleration sections in order to maximize user potential. Plotted is both the horizontal (black) and vertical (red) normalised emittance.
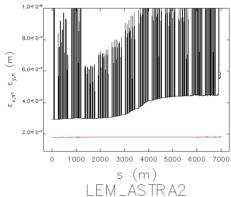
Figure 10: Start-to-end emittance plot for the LEM.

The horizontal plane follows the same fate as previously discussed, with the emittance growth mainly due to incoherent radiation, whereas the vertical values relatively remain constant until the small wavering in the final stages due to the increase in energy spread Fig. 11 during deceleration. Neglecting the correlated content the energy spread increase factor is approximately given by the ratio of the energy on deceleration $E_{in}/E_{out} = 24$.
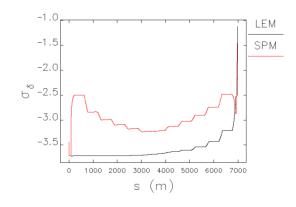
Figure 11: Log plot of the energy spread for both modes.

Short Pulse Mode Recovery Scheme

The complicated SPM relies on off-crest acceleration and deceleration, achromatic Arcs with telescopic $\mp R_{56}$ (de)compression and the charge dependent, bunch length limiting effects from coherent radiation is discussed here.
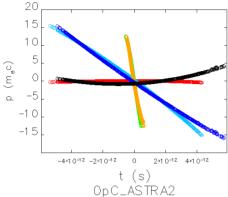

Figure 12: Long. phase space plots (2nd order theory).

Fig. 12 shows the theory of the telescopic compression without radiation effects during acceleration (red, light blue, green) in the first two Arcs up to a beam energy of 2 GeV using off-crest acceleration $\phi_1 = +10\,^\circ$, $\phi_2 = -20\,^\circ$ and positive R_{56} values in both Arcs. Also shown is the symmetric deceleration (orange, dark blue, black) from 2 GeV back to the preinjector for an ASTRA input bunch. On recovery the phase space plots are made to overlap and follow the trend used during acceleration by setting $\phi_{1,2} \to \pi^c$ so that $\phi_1 = 190\,^\circ$, $\phi_2 = 160\,^\circ$ and creating optic with negative R_{56} values.
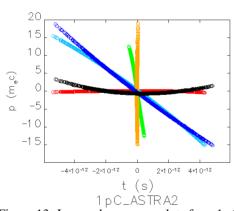

Figure 13: Long. phase space plots for a 1 pC beam.

However in reality, when radiation effects are taken into account, the recovery is not perfect. The increase in energy spread, Fig. 13 (orange compared to green) during the high energy passes requires a slightly modified optic to match the final beam properties during decompression. It is also envisaged that multipoles can once again be used in the deceleration stages to correct the 2nd order effects or enhance the chromaticity[14] to suppress beam breakup. The suitability of this optic is still under investigation.

Table 5: Simulation results at the Beam Dump entrance

Type	ε_{nx} (mm mrad)	ε_{ny} (mm mrad)	St (ps)	$\Delta E/E$ (%)	Charge (pC)
SPM	0.48	0.20	2.24	3.76	1
LEM	0.36	0.18	4.02	7.60	15

Simulation results of the recovery of the beam to the dump are given in Table 5. Although the energy spread of the beam in both modes at the entrance to the dump line is approximately 5%, the beam could be safely transported to the dump using a low dispersive optic.

REFERENCES

[1] Y. Petenev et al., "Multi-Turn ERL Based Light Source: Analysis of Injection and Recovery Schemes", IPAC2013, China.

[2] J. Knobloch et al., Status of the BERLinPro Energy Recovery Linac Project, IPAC 2012, New Orleans, July 2012.

[3] T. Atkinson et al., "Feasibility Study of Short Pulse Mode Operation for Multi-Turn ERL light source", Linac12, Israel.

[4] Ya.S. Derbenev et al., "Transerve Effects of Microbunch Radiative Interaction", SLAC Report 7181, 1996.

[5] R.D. Ryne et al., "Large Scale Simulation of Synchrotron Radiation Using a Lienard-Wiechert Approach", IPAC 2012, New Orleans.

[6] J. Wu et al., PAC 2001, p.2866-2868.

[7] CSRtrack, http://www.desy.de/fel-beam/csrtrack/index.html.

[8] S.Di Mitri et al., "Cancellation of Coherent Synchrotron Radiation Kicks with Optic Balance", Physical Review Letters 110,014801,2013

[9] ASTRA code, A Space Charge Tracking Algorithm, http://tesla.desy.de/ meykopff/ 2012.

[10] M. Borland, "elegant: A Flexible SDDS-Compliant Code for Accelerator Simulation", Advanced Photon Source LS-287, September 2000.

[11] Z. Huang et al, "Measurement of the LCLS laser Heater and its impact on the x-ray FEL performance", SLAC-PUB-13854

[12] E. Pozdeyev, "Regenerative multipass beam breakup in two dimensions", Phys. Rev. ST AB 8, 054401

[13] E.L. Saldin et al, "On the Coherent Radiation of an Electron Bunch Moving in an Arc of a Circle", TESLA FEL 1996.

[14] V. N. Litvinenko, "Chromaticity of the lattice and beam stability in energy recovery linacs", Phys. Rev. ST AB 15, 074401 (2012)